J. Fluid Mech. (1986), *vol.* 164, *pp.* 53–76
Printed in Great Britain

Maximal two-layer exchange over a sill and through the combination of a sill and contraction with barotropic flow

By D. M. FARMER
Institute of Ocean Sciences, Sidney, BC, Canada, V8L 4B2
AND L. ARMI
Scripps Institution of Oceanography, La Jolla, California 92093

(Received 14 January 1985 and in revised form 8 July 1985)

The analysis of two-layer exchange flow through contractions with a barotropic component treated by Armi & Farmer (1986) is extended to include exchange flows over sills and through a combination of a sill and contraction. It is shown that exchange over a sill is fundamentally different from exchange through a contraction. Control at the sill crest acts primarily through the deeper layer into which the sill projects and only indirectly controls the surface layer. This asymmetry in the control results in asymmetrical flows. The interface depth above the crest is not one half the total depth, as assumed in other studies by analogy with flow through contractions, but is somewhat deeper; the maximal exchange rate is less than for flow through a contraction of equal depth. When both a sill and a contraction are present, the contraction influences control at the sill crest only if it lies between the sill and the source of denser water. The response to barotropic flow is also asymmetrical: the transition to single-layer flow occurs at much lower speeds for a barotropic component in one direction than the other.

Results of the analysis are applied to exchange flow through the Strait of Gibraltar, which includes both a sill and a contraction. It is shown that maximal exchange conditions apply throughout part of the tidal cycle, and observations illustrate several of the analytical predictions for barotropic flows, including the formation of fronts, single-layer flow, submaximal exchange and reverse flow.

1. Introduction

The exchange of two fluids of different density in a channel of constant width is a well-established topic of fluid mechanics with a wide range of applications (see for example Turner 1973). We consider here a modification of this 'lock-exchange' problem in which a sill on the floor of the channel influences the maximal two-layer exchange. Two-way exchange over a sill differs in a fundamental way from the corresponding example of two-way exchange through a contraction (which is discussed in the companion paper by Armi & Farmer 1986), in that the sill only projects into the deeper fluid so that the hydraulic control acts on the total exchange flow primarily through its effect on the deeper layer.

Maximal two-way exchange constitutes the steady-state limit that occurs when fluids of differing density are free to move in opposite directions across the sill. Sills are a common feature of channels separating deep estuaries and semi-enclosed seas from the open ocean and the overmixing solution for flows through contractions identified by Stommel & Farmer (1953) has often been invoked to explain the

consequences of this exchange to the local oceanography (see, for example, Anati 1976; Bryden & Stommel 1984; Hogg 1985; Murray, Hecht & Babcock 1984; Stigebrandt 1977). However, we shall show that, in contrast to exchange through a horizontal contraction, these applications of the special solution found by Stommel & Farmer are incorrect, since they are not applicable to maximal two-layer exchange over a sill.

The analysis is extended to include barotropic flows such as might be induced by meteorological effects or tides, in which we consider quasi-steady flows where the internal hydraulic adjustments are rapid compared with the forcing. Finally we extend the analysis to include the combination of a sill and a horizontal contraction and consider both the case in which a sill and a contraction are separated and the case in which they are coincident. The solutions are integrated so as to determine the maximal exchange when averaged over a tidal cycle. These solutions are applicable to a broad class of naturally occurring flows in straits and channels.

2. Basic assumptions and flow configuration

Figure 1 shows the flow configuration with which we are concerned. Initially we consider a channel that is of uniform width separating two broad and deep reservoirs which, except in the neighbourhood of the sill, is sufficiently deep that the speed of the thicker layer is negligible away from the influence of the sill. This latter condition is easily relaxed (cf. §7) but serves to isolate the essential physics of the control. In the figure the source of less dense fluid is on the left. In an oceanographic application this less dense fluid might correspond, for example, to a fresh layer produced by river discharge into a deep estuary or alternatively an ocean inflow moving into an inverse estuary such as the Mediterranean in which the effect of evaporation exceeds that of precipitation. The corresponding source of deep denser fluid is on the right.

In figure 1 we have shown the sill lying within a relatively short section of the channel separating each reservoir. However, our discussion is equally applicable to a sill lying in a channel of infinite length and uniform width. In this highly idealized and unrealistic case, however, the reservoir to the right of the channel would have a surface layer that approached critical conditions asymptotically with distance from the sill crest. In practice frictional effects would dominate in a very long, uniform channel. As discussed in detail subsequently, the exit to the reservoir, b_e, acts as a control on the surface layer and effectively isolates the hydraulic processes under discussion from frictional, mixing and other effects that might be relevant in the reservoir itself.

In the following discussion we assume that the flow is inviscid and each layer is homogeneous and unsheared, as in Armi & Farmer (1986). Mixing between the layers between the the sill crest and the exit b_e is neglected, although mixing may well be an important feature outside this region. To the left of the sill crest in figure 1, the dense water runs down the slope where it may either be matched to a reservoir interface through an internal hydraulic jump, or may separate from the sill or merge with the fluid in the deep basin in some other way. We shall show subsequently that, over a wide range of interface depths in the reservoirs, the details of this process do not influence two-way exchange over the sill crest. The surface layer is matched to conditions in the reservoir to the right, outside the straight section.

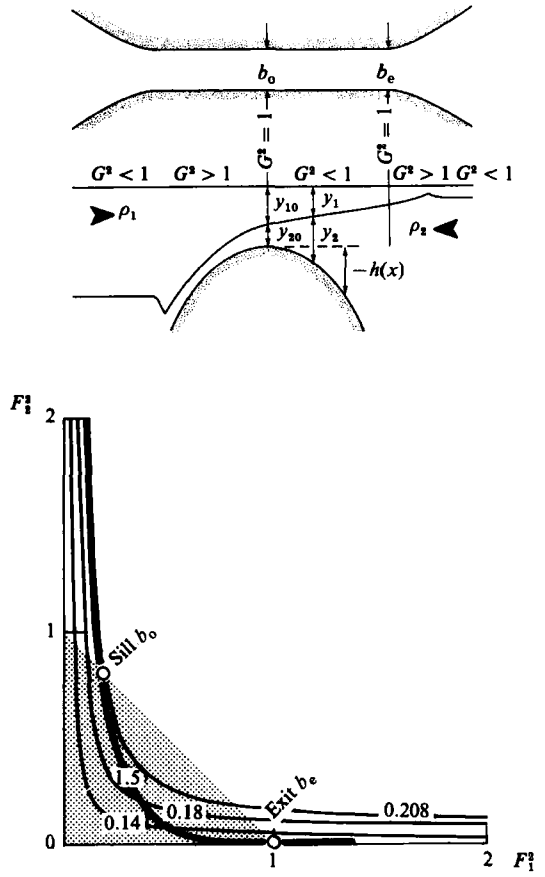

FIGURE 1. *Above.* Side and plan views for maximal two-layer exchange flow, showing position of the interface. *Below.* Froude-number plane showing solution to (12) for maximal two-layer exchange (heavy line). The position of the sill (b_0), and exit (b_e) in this plane are shown as circles. The light lines correspond to solutions of the continuity equation (7) and the subcritical region is shaded. Note that the flow is critical ($G^2 = 1$) at b_0 and b_e.

3. Two-way exchange over a sill and representation in the Froude-number plane

We are concerned with two-way exchange between reservoirs containing fluids of differing density ρ_1, ρ_2, subject to hydraulic control by a sill. Except in the trivial case of zero exchange, the interface will always be asymmetrical when the flow is controlled and thus subject to an internal hydraulic transition as the flow changes from subcritical to critical (Armi 1986). For two layers the flow is said to be critical at locations for which

$$G^2 = F_1^2 + F_2^2 = 1 \quad (g' \ll g), \tag{1}$$

where $F_i^2 = u_i^2/g'y_i$ is the densimetric Froude number for layer i, u_i is the flow speed, y_i the layer thickness and $g' = g\,\Delta\rho/\rho_2$ is the reduced gravity ($\Delta\rho = \rho_2 - \rho_1$). The upper and lower layers are identified by $i = 1$, $i = 2$ respectively; where possible the notation and figures correspond to their equivalents in Armi & Farmer (1986).

The composite Froude number G^2 characterizes the essential nonlinearity of the

flow and solutions are thus expressed in terms of F_1^2, F_2^2. Figure 1 shows a solution (the solid line) in the Froude-number plane, in which condition (1) collapses to a straight line.

The flow rate $q_i = y_i u_i b$ is expressed in non-dimensional form as

$$q_i' = \frac{q_i}{g'^{\frac{1}{2}}(y_1+y_2)_0^{\frac{3}{2}}}, \tag{2}$$

where $(y_1+y_2)_0$ is the total water depth at the sill crest and b is the channel breadth, initially taken as constant. The depth of the channel $-h(x)$ is measured with reference to the depth of the sill crest ($h_0 = 0$, see figure 1). The corresponding dimensionless depth is

$$h' = \frac{h}{(y_1+y_2)_0}, \tag{3}$$

and the dimensionless layer thickness is

$$y_i' = \frac{y_i}{(y_1+y_2)_0}. \tag{4}$$

The rigid-lid approximation, which is well justified for these flows in which the external Froude number is very small, may be expressed as

$$y_1'+y_2'+h' = 1. \tag{5}$$

Using the above definitions of q_i', F_i^2, y_i' and h', the dimensionless-layer depth may be expressed as

$$y_i' = (q_i')^{\frac{2}{3}} F_i^{-\frac{2}{3}}. \tag{6}$$

Throughout this paper we adopt the convention that flow in the upper layer is positive and thus, for exchange flows, lower-layer speeds are negative. The ratio of flow rates in each layer is defined as $q_r = q_1/-q_2$, so that in steady flow between two homogeneous reservoirs without barotropic flow $q_r = 1$.

We restrict attention to the quasi-steady example for which the flow rates q_i are independent of position along the channel. Then (5) and (6) constitute the continuity conditions, which may be combined to yield the continuity condition in Froude-number space:

$$q_r^{\frac{2}{3}} F_1^{-\frac{2}{3}} + F_2^{-\frac{2}{3}} = \left[\frac{q_2'}{(1-h')^{\frac{3}{2}}}\right]^{-\frac{2}{3}}. \tag{7}$$

For given q_r, contours of constant $q_2'/(1-h')^{\frac{3}{2}}$ may be plotted as a function of F_1^2, F_2^2. Figure 1 (*b*) shows two contours of this quantity for $q_r = 1$, plotted as light lines.

The Bernoulli equations for each layer are

$$H_1 = \tfrac{1}{2}\rho_1 u_1^2 + \rho_1 g(y_1+y_2+h)+p, \tag{8}$$

$$H_2 = \tfrac{1}{2}\rho_2 u_2^2 + \rho_1 g y_1 + \rho_2 g(y_2+h)+p, \tag{9}$$

where p is the pressure at the surface. Subtracting (9) from (8), dividing through by $g'\rho_2(y_1+y_2)_0$ and making use of the continuity equation (7), we express the dimensionless Bernoulli equations in Froude-number space:

$$\frac{H_1-H_2}{g'\rho_2(y_1+y_2)_0} = \tfrac{1}{2}\frac{\rho_1}{\rho_2} y_1' F_1^2 - \tfrac{1}{2} y_2' F_2^2 - (y_2'+h'). \tag{10}$$

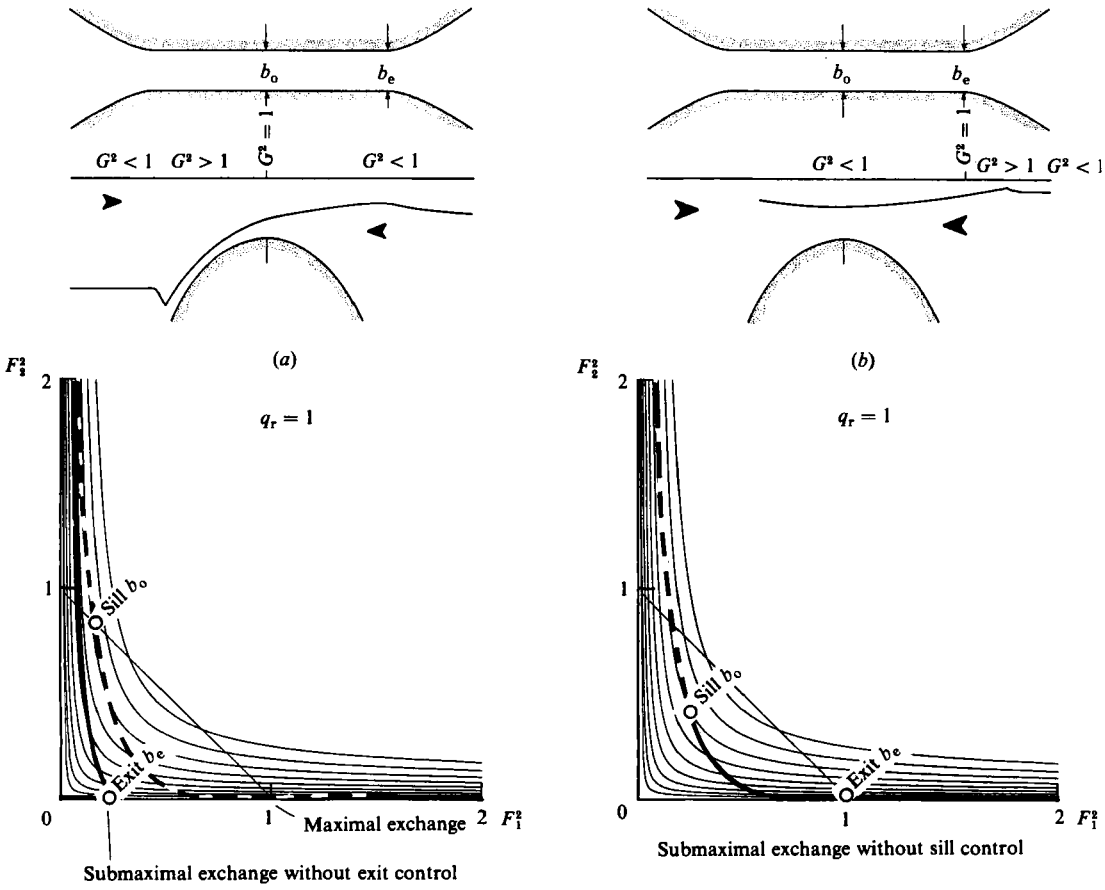

FIGURE 2. (*a*) *Above.* Sketch showing plan view and interface shape for submaximal exchange with critical conditions at the sill crest but subcritical flow at the exit. *Below.* Froude-number plane showing a solution curve (heavy line) corresponding to the submaximal flow sketched above. The maximal-exchange solution is also shown (dashed line) for comparison. (*b*) *Above.* Sketch showing plan view and interface shape for submaximal exchange with critical conditions at the exit but subcritical flow at the sill crest. *Below.* Froude-number plane showing a solution curve (heavy line) corresponding to the submaximal flow sketched above, illustrating critical flow at the exit b_e and subcritical flow over the crest b_0. The solution is coincident with a portion of the maximal-exchange solution although not extending to critical conditions at the crest; the extension of the maximal curve is shown as a dashed line.

The rigid-lid approximation (5) allows (10) to be written

$$\frac{H_1 - H_2}{g'\rho_2(y_1+y_2)_0} + 1 = \Delta H'' = y_1'(1+\tfrac{1}{2}F_1^2) - \tfrac{1}{2}y_2'F_2^2. \tag{11}$$

Combining (11) and (6) yields

$$F_2^2 = q_r[2F_1^{-\frac{2}{3}} + F_1^{\frac{4}{3}} - 2\Delta H'' q_1'^{-\frac{2}{3}}]^{\frac{3}{2}}. \tag{12}$$

Solutions, expressed in terms of the parameter $\Delta H'' q_1'^{-\frac{2}{3}}$, are plotted as a function of F_1^2, F_2^2 in figures 1, 2, and 3 (see also Armi 1985), using heavy lines. The lighter lines are contours satisfying the continuity condition (7).

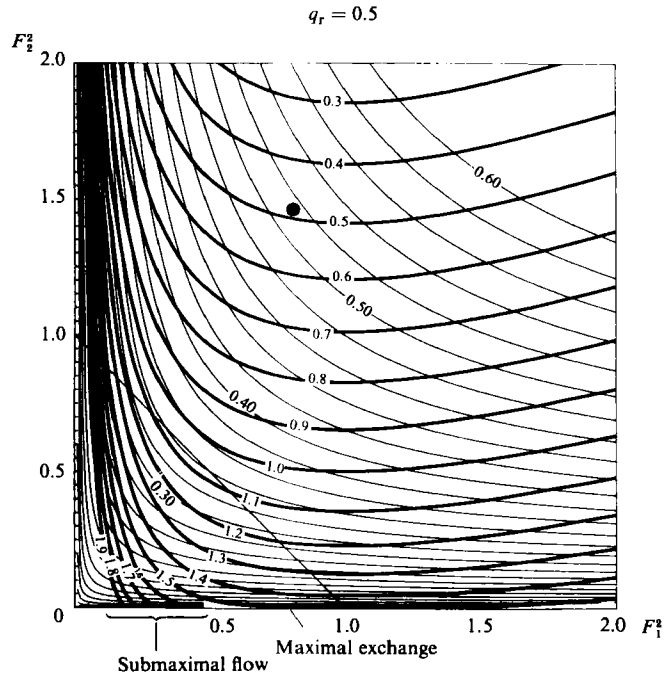

FIGURE 3. Solution curves in the Froude-number plane (from Armi 1985) with barotropic flow ($q_r = 0.5$). These solutions apply also to flows in the same direction as well as to the exchange flows treated here. Only that portion of the maximal exchange solution for which $F_1^2 \geqslant 1$ is relevant.

4. Maximal two-layer exchange flows

Solutions applicable to an infinitely deep reservoir (i.e. on the right side of the sill in figure 1) must intersect the horizontal axis, since $F_2^2 = 0$ in the reservoir to the right. Calculation of these solutions (i.e. $\Delta H'' q_1'^{-\frac{2}{3}}$ as a function of F_1^2, F_2^2), as well as inspection of figure 1, shows that the solution curve, plotted as a heavy line, which passes through $G^2 = 1$ at the crest *and* which is identified with the maximal exchange rate ($q_2' = 0.208$ plotted as a light line in the figure) is the only one that also matches the reservoir condition $F_1^2 = 1$, $F_2^2 = 0$. This unique solution is evaluated from (12):

$$\Delta H'' q_1'^{-\frac{2}{3}} = \tfrac{3}{2}. \tag{13}$$

This result is equally applicable for barotropic flows, since it is independent of q_r and is the only specific solution in the plane corresponding to maximal two-way exchange.

The interface shape in figure 1 may now be interpreted in terms of the maximal-solution curve plotted in the Froude-number plane. Critical conditions occur at the sill crest b_0 and also at the exit b_e. Between these two controls the flow is subcritical (shaded region in Froude-number plane). To the left of the sill crest the lower layer accelerates down the sill as a supercritical flow ($G^2 > 1$). Eventually this supercritical flow is matched to the left-hand reservoir interface through an internal hydraulic jump or by some other process; these details, however, are unimportant to the exchange conditions since they are isolated from the control region by the supercritical flow. To the right of the exit b_e the surface layer accelerates ($G^2 > 1$) and is eventually matched to the right-hand reservoir interface. In the Froude-number plane the solution for this portion of the flow is just a straight line running along the axis $F_2^2 = 0$.

In this way the supercritical flows on either side of the control section serve to isolate the maximal exchange flow from the reservoir interface positions. This physical isolation of the exchange process underlies the importance of the maximal exchange solution, since the global problem of movement of fluid between the two reservoirs is fully determined, regardless of detailed processes occurring outside the control section.

The interface height y'_{2o} at the sill crest for the maximal exchange solution may be solved from the corresponding values of F_1^2 and F_2^2 satisfying (11) and (1) and is found to be

$$y'_{2o} = 0.375. \tag{14}$$

This result differs significantly from the corresponding maximal exchange interface height,

$$y'_{2o} = 0.5, \tag{15}$$

found by Stommel & Farmer (1953) and discussed by Armi & Farmer (1985*a*) for the flow through a horizontal contraction. Thus, previous applications of Stommel & Farmer's solution to two-way exchange over a sill are incorrect.

Submaximal exchanges are also possible. The exchange rates for these solutions are less than the maximal solution (i.e. $q'_2 < 0.208$) and in contrast to the maximal exchange are not isolated from both of the reservoir conditions. These solutions arise when the interface level in the left-hand reservoir is sufficiently shallow, or in the right-hand reservoir is sufficiently deep, to override one of the two controls. Figure 2 (*a*) illustrates the case when the right-hand reservoir interface is deep enough to flood the exit control b_e. This solution is shown beneath in the Froude-number plane and is seen to intersect the $F_2^2 = 0$ axis at $F_1^2 < 1$. The intersection of the solution with $G^2 = 1$ at the sill crest corresponds to a lower exchange rate than for the maximal solution, which is also shown.

The opposite submaximal example is shown in figure 2 (*b*). In this case the interface in the left-hand reservoir is shallow enough to flood the sill crest control. The solution in the Froude-number plane passes through $G^2 = 1$ at the exit b_e ($F_2^2 = 0$), but does not reach critical conditions at the sill crest and is therefore identified with a correspondingly lower exchange rate. The precise shape of the interface near the exit to the left-hand reservoir will be governed by interfacial friction and will not be discussed here. The limits on interfacial positions within which maximal solutions can occur are given in §7.

5. Moderate barotropic exchange flows over a sill

The effect of a barotropic component on the exchange flow can be expressed in terms of the ratio of flow rates q_r. Figure 3 shows solutions for $q_r = 0.5$. In contrast to flow through horizontal contractions, the introduction of moderate barotropic flow introduces no qualitative change to the solutions; in particular, a 'virtual' control does not appear since the position of the second control is already fixed at the right-hand exit of the channel, b_e. The solution curves are shifted, in this case toward higher F_2^2 values at the sill, reflecting the relatively greater flow rate in the lower layer implied by our choice of $q_r = 0.5$. However, the maximal solution, which is tangent to the horizontal axis at $F_1^2 = 1$, has the same value ($\Delta H'' q_1'^{-\frac{2}{3}} = \frac{2}{3}$) as before.

The equations for barotropic flow over a sill are similar to those applicable to a horizontal contraction, except that the virtual control condition is replaced by an exit control at b_e, which for an infinitely deep reservoir acts only on the surface layer.

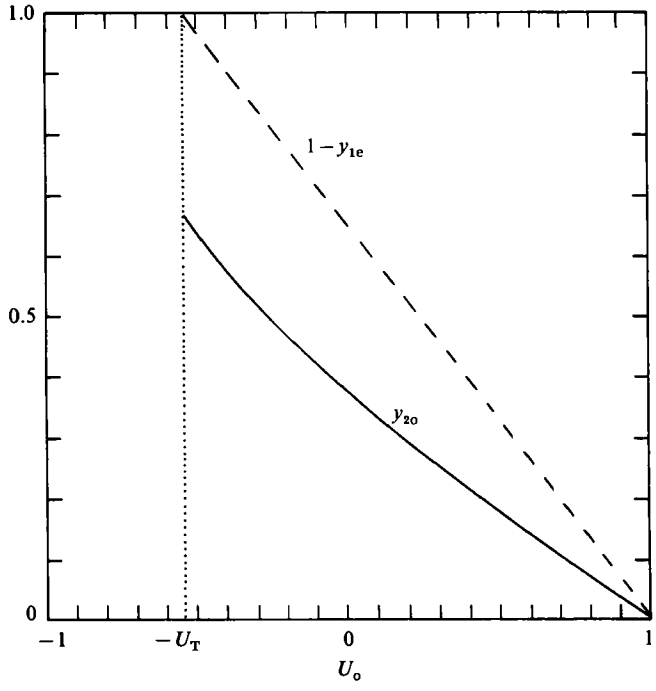

FIGURE 4. Interface height above the sill crest y_{2o}, and at the exit, $1-y_{1e}$, as functions of the barotropic flow, U_o.

For the moderate barotropic exchange flows discussed here, control is retained at both the sill crest and at the exit, so that the general shape of the interface remains similar to that sketched in figure 1. The effect of the barotropic component is to modify to some extent the interface heights within the control section together with the corresponding layer speeds and flow rates. On dropping the primes, the control condition at the crest becomes

$$\frac{u_{1o}^2}{y_{1o}}+\frac{u_{2o}^2}{y_{2o}}=1, \tag{16a}$$

and the definition of water depth at the sill crest is

$$y_{1o}+y_{2o}=1, \tag{16b}$$

where the flow speeds are non-dimensionalized with $\sqrt{(g'(y_1+y_2)_o)}$. The relevant energy equation at the two controls is

$$\tfrac{1}{2}(u_{2o}^2-u_{1o}^2)+y_{2o}=\tfrac{1}{2}(u_{2e}^2-u_{1e}^2)+(y_{2e}-h), \tag{16c}'$$

which immediately reduces to

$$\tfrac{1}{2}(u_{2o}^2-u_{1o}^2)-y_{1o}=-\tfrac{1}{2}u_{1e}^2-y_{1e}. \tag{16c}$$

The exit condition is

$$\frac{u_{1e}^2}{y_{1e}}=1, \tag{16d}$$

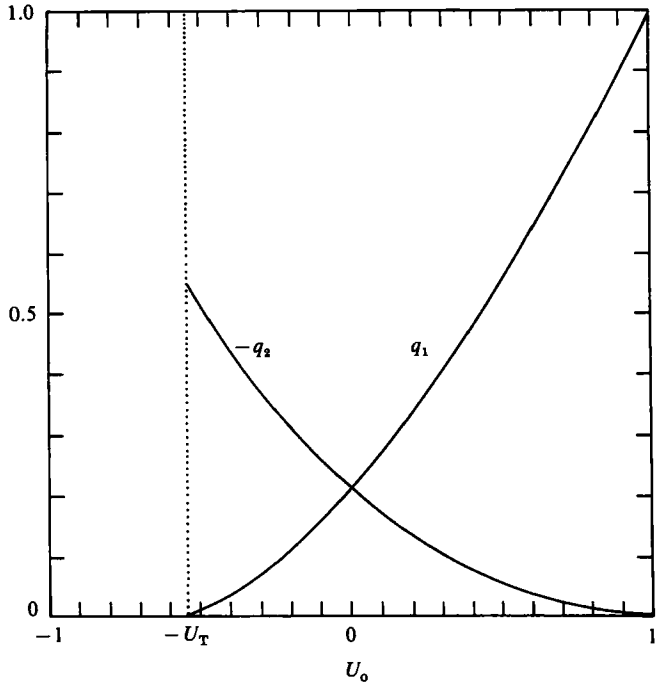

FIGURE 5. Volume flow rates q_1 and q_2 as functions of U_0 for moderate barotropic flow.

and the continuity equation is

$$u_{1o} y_{1o} = u_{1e} y_{1e}. \tag{16e}$$

We define the barotropic flow as

$$U_0 \equiv u_{1o} y_{1o} + u_{2o} y_{2o}. \tag{16f}$$

We now examine solutions to the system of equations (16*a–f*) within these limits, which we refer to as moderate barotropic exchange flows.

In figure 4 we plot solutions of the interface height relative to the sill crest at the control y_{2o} and at the exit control b_e, as a function of U_0. Comparison with the corresponding result for flow through a horizontal contraction shows that y_{2o} for flow over a sill is always less, except at the limit $U_0 = -U_T$. The existence of a stationary layer at the sill crest is only possible for negative barotropic forcing (from right to left); at the positive limit $U_0 = 1$, the surface layer fills the channel at the sill crest.

The flow rates over the sill (see figure 5) are similar, though not identical with, the equivalent results for a contraction. In the absence of barotropic forcing, maximal exchange over a sill occurs for a flow rate only 0.832 that for maximal exchange through a contraction. The dependence of exchange rate on barotropic forcing is also less linear for the sill flow than for flow through a contraction, which will have consequences for the corresponding parametrization of periodic forcing (§7).

The asymmetry of the barotropically forced sill flow is even more striking with respect to the flow speeds and shear at the sill crest (Δu_0), shown in figure 6. The flow speeds in each layer are equal and opposite at a positive barotropic flow speed ($U_0 = 0.196$) and the shear at the crest increases monotonically from $U_0 = -U_T$ to $U_0 = 1$. In contrast to flow through a horizontal contraction, marginal stability

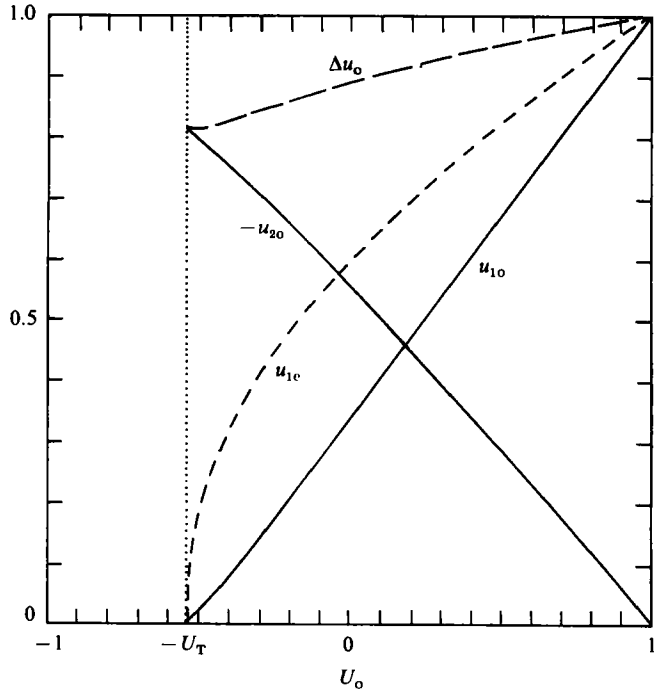

FIGURE 6. Velocities at the sill crest, u_{10} and u_{20}, as well as for the surface layer at the exit, u_{1e}, as functions of U_0 for moderate barotropic flow. Note that the velocity difference $\Delta u_0 = u_{10} - u_{20}$ at the sill crest is always less than one, implying stable flow.

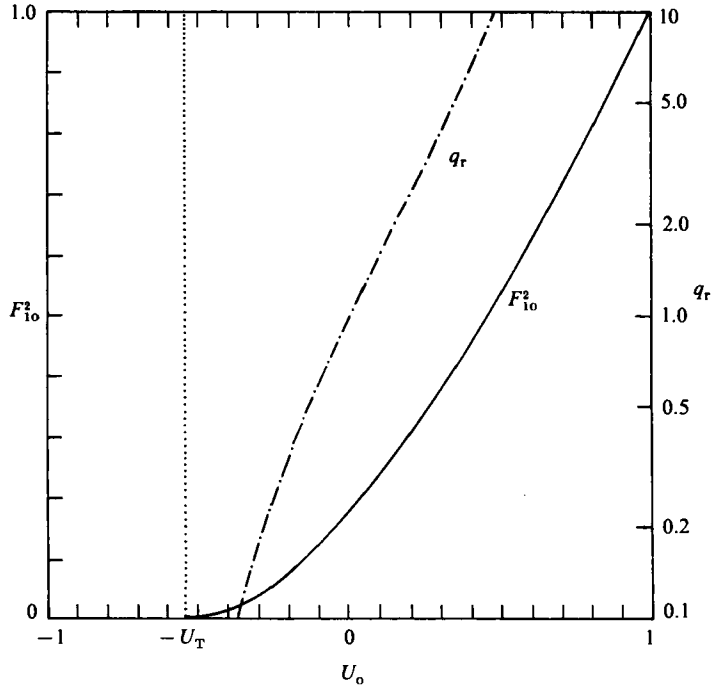

FIGURE 7. The flow ratio, q_r, and surface-layer Froude number F_{10}^2, at the sill crest as functions of U_0 for moderate barotropic flow.

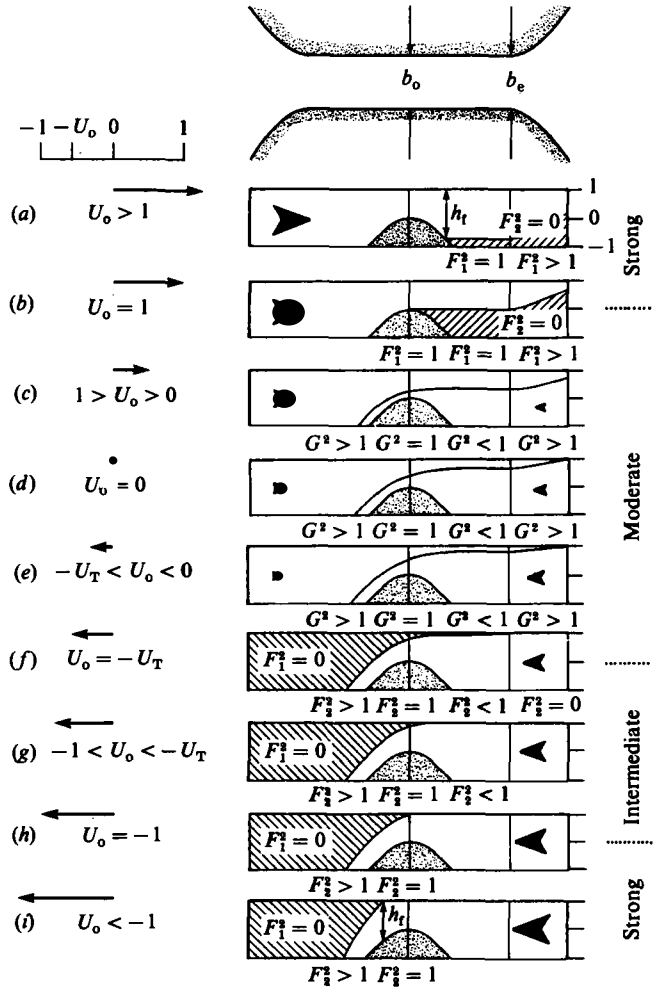

FIGURE 8. Sketches of the interface positions as a function of barotropic flow U_0. The arrows to the left of the sketches indicate the strength and direction of the barotropic component; the arrowheads within each sketch indicate direction and magnitude of flow rate for each layer. Motionless layers are shaded. Layer Froude numbers F_i^2 and composite Froude numbers G^2 are indicated beneath each sketch.

($\Delta u_0 = 1$) does not occur in the absence of barotropic forcing, so that the reason put forward by Stommel & Farmer (1952) for choosing the control condition at the narrowest section, would not apply to exchange flow over a sill. The Froude number for the surface layer at the sill crest is also consistently less than the corresponding value for a horizontal contraction. F_{1o}^2 and q_r are plotted in figure 7; $F_{1o}^2 = 0.177$ in the absence of barotropic forcing, compared with 0.25 for the contraction (equation (11) in Armi & Farmer 1986).

These solutions for moderate barotropic exchange flows are summarized in the central sketches of figure 8 (*c*, *d*, *e*). For a barotropic flow from left to right (figure 8*c*) the interface drops, consistently with figure 4; the interface rises for barotropic flow from right to left (figure 8*e*). The moderate barotropic solutions shown in figures 4–7

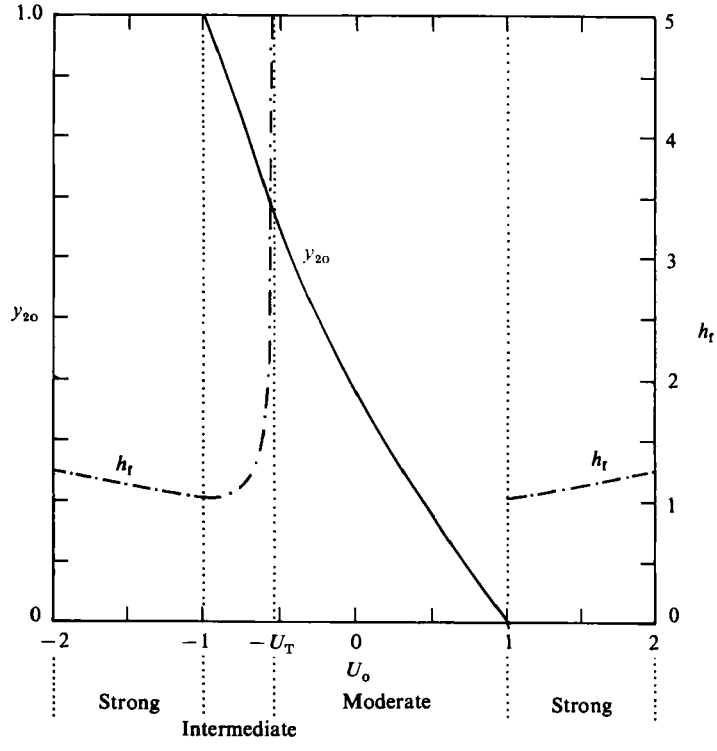

FIGURE 9. Interface height y_{20} above sill crest and total fluid depth h_t at the transition between single and two-layer fluid, for intermediate and strong barotropic flow. For $U_0 > 1$ the interface intersects the bottom; for $-1 < U_0 < -U_T$ it intersects the surface to the right of the sill and for $U_0 < -1$ to the left.

span the range $-U_T \leqslant U_0 \leqslant 1$. The limiting values correspond to flows in which the barotropic component is just sufficient to arrest one of the two layers. These limiting cases for positive and negative barotropic flow are shown in figures 8(*b*) and (*f*) respectively.

For barotropic flow from right to left, the limiting condition $-U_T$ is found from (16*a*, *b*, *c*):

$$-U_T = -(\tfrac{2}{3})^{\frac{3}{2}}, \tag{17}$$

at which point $y_{20} = \frac{2}{3}$ and $u_{20} = (\frac{2}{3})^{\frac{1}{2}} = 0.81$. Unlike flow through a contraction, however, this limiting condition is not symmetrical and is discussed further in §6. For positive barotropic flow the corresponding limit is

$$U_0 = 1. \tag{18}$$

6. Intermediate and strong barotropic forcing

Barotropic flows for which $U_0 < -U_T$ or $U_0 > 1$ are associated with a single moving layer; we refer to these flows as intermediate or strong to distinguish them from two-way exchange solutions discussed in §4. Sketches of the interface shape through a progression of different barotropic regimes, such as might be encountered through a tidal cycle, are shown in figure 8.

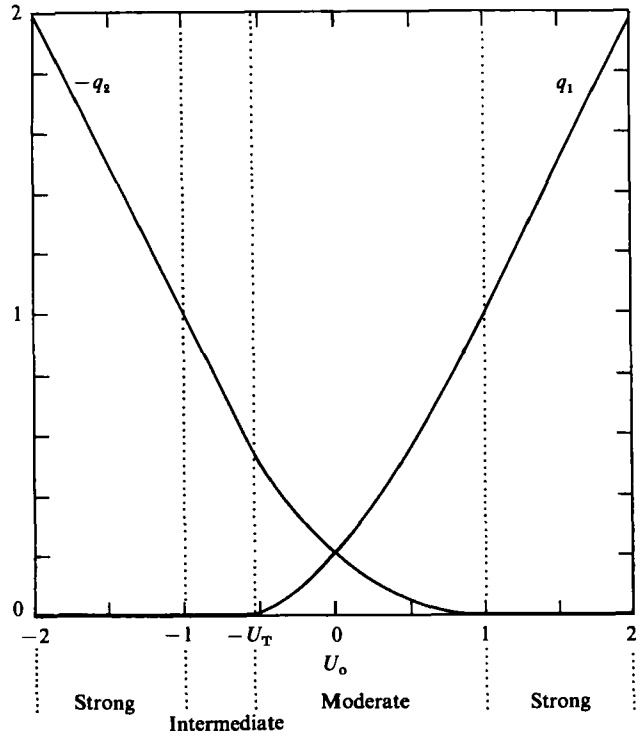

FIGURE 10. Flow rates q_1, q_2 for moderate, intermediate and strong flow.

Figure 8(*d*) shows the two-way exchange for $U_0 = 0$; figure 8(*c*) and (*e*) show moderate barotropic flow from the left and right respectively. The limiting flow from the left (i.e. equation 18), is shown in figure 8(*b*). The surface layer fills the channel at the sill crest and the interface is horizontal in the reservoir to the right. Thus the surface-layer Froude number is $F_1^2 = 1$ to the right of the crest and the lower layer is blocked. Further increase in the barotropic component will increase the depth of intersection with the sill, h_f (figure 8*a*), so as to maintain the exit condition (16*d*):

$$h_f = U_0^{\frac{2}{3}}. \tag{19}$$

For flow from right to left, the transition to intermediate flows, with the arrest of the surface layer, occurs at $U_0 = -U_T = -(\frac{2}{3})^{\frac{3}{2}}$ shown in figure 8(*f*). Increased barotropic flow causes a front to form upstream of the sill crest. The front location, in terms of local channel depth h_f, is found by eliminating u_{to}, y_{to} from the energy equation (16*c*) and making use of the identity $U_0 = u_{2f} h_f$:

$$h_f = U_0(3U_0^{\frac{2}{3}} - 2)^{-\frac{1}{2}}. \tag{20}$$

The front passes over the crest at $U_0 = 1$, above which value the flow is in the strong regime (see figure 8*h*, *i*). Further increase in U_0 causes the channel depth at the front to vary linearly with the flow:

$$h_f = U_0. \tag{21}$$

Plots of the interface heights, flow rates and flow speeds, corresponding to the full range of flow regimes sketched in figure 8, are shown in figures 9, 10 and 11

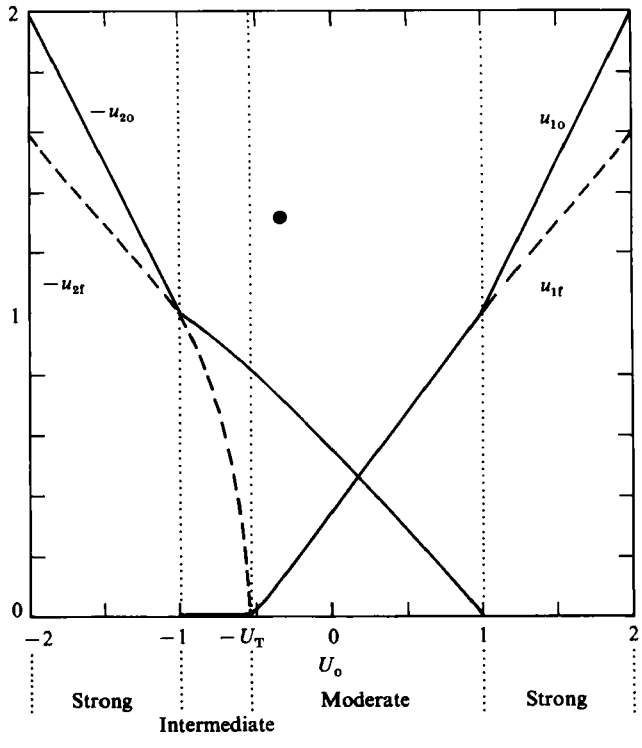

FIGURE 11. Layer speeds u_{1o}, u_{2o} at the sill crest, and layer speeds u_{1f}, u_{2f} at the transition between single and two-layer conditions.

respectively. Figure 9 also shows the location h_f of the intersection with the sill ($U_0 > 1$) and of the intersection with the surface ($U_0 < U_T$). Note the very great sensitivity of the frontal position to the strength of the barotropic flow when U_0 is close to $-U_T$; in natural flows we anticipate the quite sudden appearance of a front upstream of the sill crest as the barotropic forcing proceeds through $-U_T$. In contrast to two-layer flows through horizontal contractions, this intermediate condition, $-U_T > U_0 > 1$, can occur only when the barotropic flow opposes the surface layer. All of the single-layer flows discussed above correspond to the box flows described by Armi & Farmer (1986), but with the control exercised by a vertical rather than a horizontal contraction.

The flow rates, q_i, vary linearly in the strong regime (figure 10) as do the flow speeds (figure 11). However, the flow speeds in this regime at the intersection point h_f vary as $U_0^{\frac{2}{3}}$; the intersection point always adjusts to maintain $F_i^2 = 1$.

7. Flows through a combination of a sill and contraction with a barotropic component

A feature of some straits is the presence of a coincident sill and contraction as shown in figure 12. This problem must in general be described by a function relating the width to the depth, rather than by parameters. As in the case of a contraction alone, there will be a control at the narrowest and shallowest section (b_0) and a virtual control whose position (b_v) will depend on the barotropic forcing. However, the behaviour of the virtual control, $b = b_v$, depends on both the width and depth. The

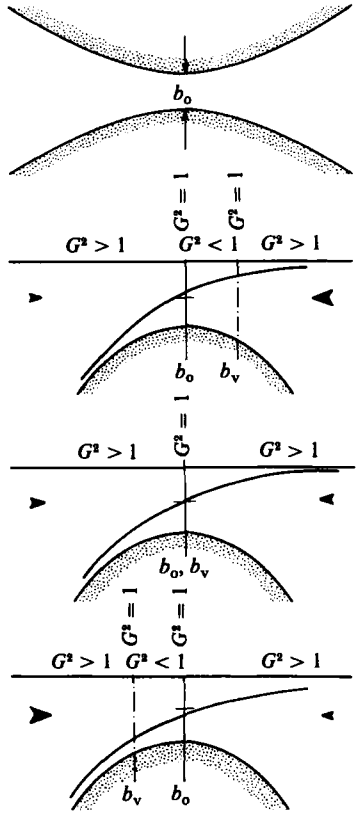

FIGURE 12. Sketch of plan view and three side views of two-way exchange past a coincident sill and contraction with moderate barotropic component. With moderate barotropic flow critical conditions occur at the narrowest and shallowest section b_0. A virtual control b_v also occurs on the upstream side of b_0, with barotropic flow; this control must always lie on the side from which the barotropic component is directed. The two controls coalesce when $U_0 = 0$.

condition at the virtual control is found from the regularity condition (see Armi 1985):

$$\left[1-\left(1+\frac{y_1}{y_2}\right)F_1^2\right]\frac{1}{b}\frac{\mathrm{d}b}{\mathrm{d}x}-[1-F_1^2]\frac{1}{y_2}\frac{\mathrm{d}h}{\mathrm{d}x}=0, \tag{22}$$

giving

$$\frac{\mathrm{d}h(b)}{\mathrm{d}b}=\frac{1-\left(1+\dfrac{y_1}{y_2}\right)F_1^2}{1-F_1^2}\frac{y_2}{b}, \tag{23}$$

which replaces (13*d*) in Armi & Farmer (1986). Similarly the total depth equation (13*e*) is replaced by

$$\frac{y_{1v}+y_{2v}}{H(b_v)}=1, \tag{24}$$

where $H(b_v)$ is the relative channel depth at b_v as defined by (27).

In the absence of barotropic flows, the two controls coalesce and the interface at the narrowest and shallowest section is half the total depth.

In many straits (for example, Gibraltar) the sill is displaced from the narrowest

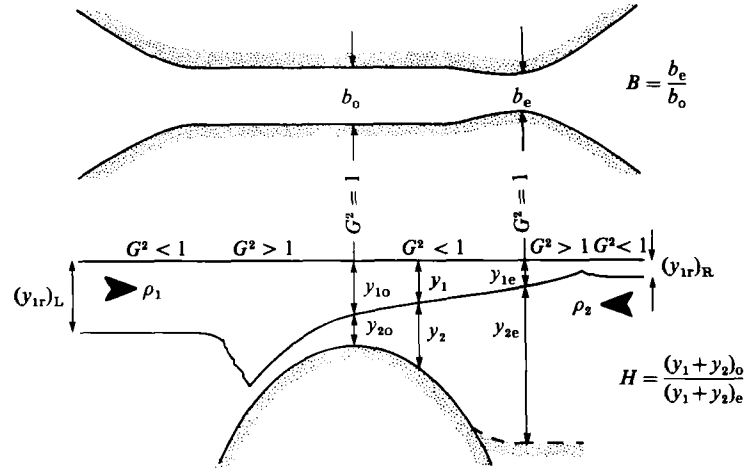

FIGURE 13. Sketch showing plan view and side view of exchange flow past a separate sill and a contraction, where B defines the ratio of width, and H the ratio of depths. Composite Froude numbers are indicated; critical conditions occur at the sill crest and at the narrowest section, which are connected by a subcritical flow. Supercritical flow outside of these two control points separates the intervening control region from conditions in the two reservoirs.

section. Consider the problem sketched in figure 13, in which a contraction exists in the deep part of the channel, to the right of the sill, where the ratio of the widths is

$$B = \frac{b_e}{b_o}. \tag{25}$$

The exit control which separates flow in the channel from the reservoir, must occur at the narrowest section where $db/dx = 0$. The equations describing two-way flow through the channel are identical to those derived in the absence of a contraction, except that the continuity equation must be modified using (25):

$$u_{1o} y_{1o} = u_{1e} y_{1e} B. \tag{16e'}$$

If the contraction were located to the left of the sill, except in the special case discussed below, it would not influence the two-way exchange. In our idealization, the channel is deep on either side of the sill, so that the control exerted by the contraction would only influence the surface layer. If, however, the contraction to the left was not much deeper than the sill crest, the control at the sill crest could be flooded, in which case two-way exchange would be governed solely by the contraction; the sill would then play no active role in the exchange and the problem would revert to that discussed by Armi & Farmer (1986).

Solutions for barotropic flow through a combination of a displaced sill and contraction (i.e. figure 13) are shown in figures 14, 15 and 16 for different values of B. The effect of reducing the width of the contraction relative to the sill is to reduce the range of positive U_0 over which two layers can coexist at the sill. Thus in figure 14, we see that, for decreasing B, the lower interface height decreases and the transition to strong forcing occurs at progressively smaller values of positive U_0. A similar effect is apparent in the flow speeds (figure 15); the corresponding flow rates are shown in figure 16. For $B = 0.1$, the transition to strong flow occurs at $U_0 = 0.05$. On the other hand, the influence of the contraction is much smaller for negative barotropic flow and the value of $-U_T$ is independent of B. This asymmetry of the influence of the

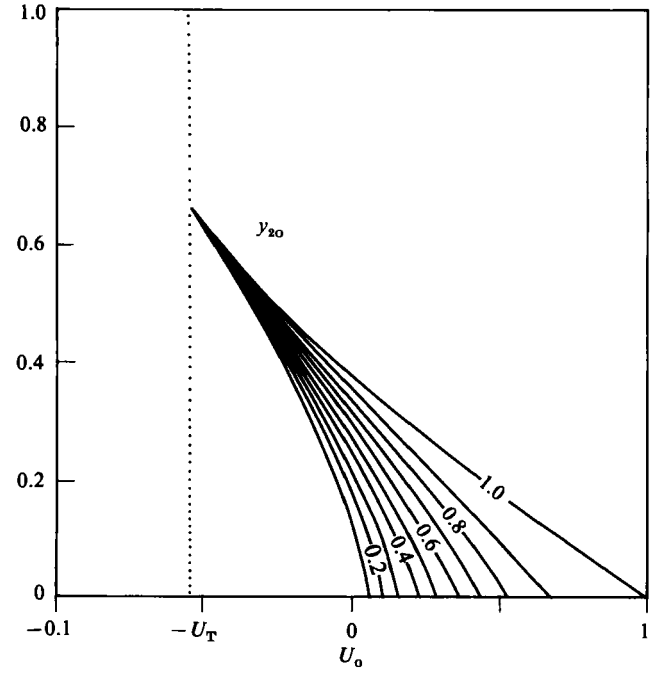

FIGURE 14. Interface heights at the sill crest y_{2o}, as a function of U_o, for different width ratios B.

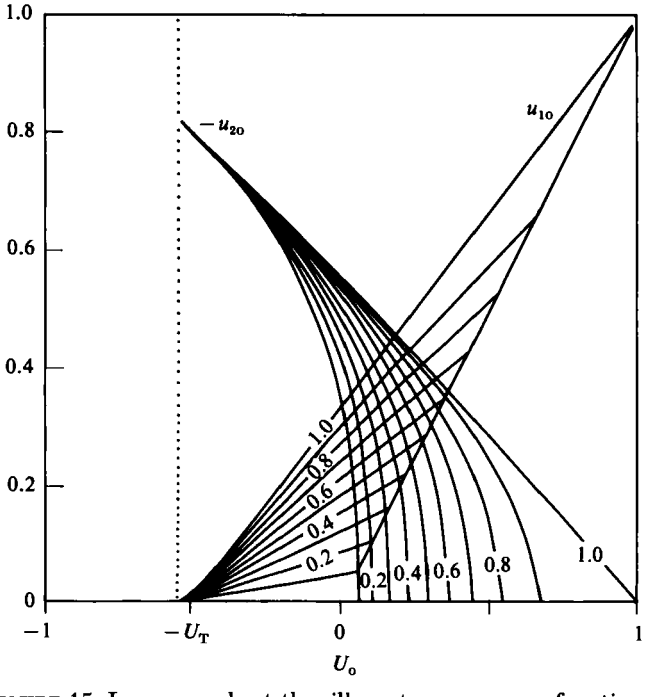

FIGURE 15. Layer speeds at the sill crest u_{1o}, u_{2o}, as a function of U_o, for different width ratios B.

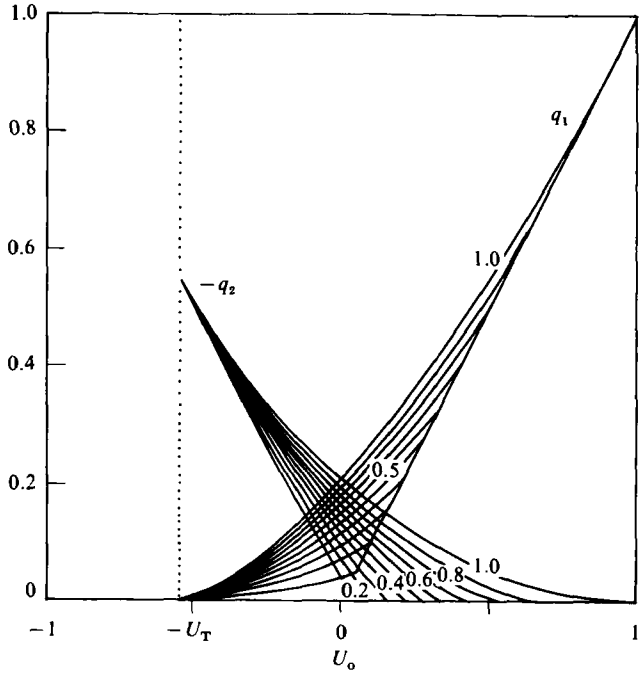

FIGURE 16. Flow rates q_1, $-q_2$, as a function of U_0, for different width ratios B.

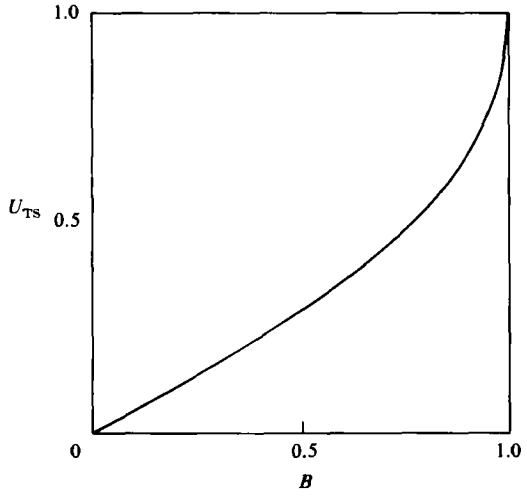

FIGURE 17. Plot showing the barotropic flow speed U_{TS} separating moderate from strong flows, as a function of width ratio B.

contraction is due to the fact that with negative barotropic component the flow in the upper layer is weak, so that the control exercised by the contraction is weak.

The value of the barotropic component, from left to right, at which there is a transition between moderate and strong flow is a function of the width ratio B. This value, $U_0 = U_{TS}$, is given implicitly by

$$B = U_{TS}(\tfrac{1}{3}U_{TS}^2 + \tfrac{2}{3})^{-\frac{3}{2}} \tag{26}$$

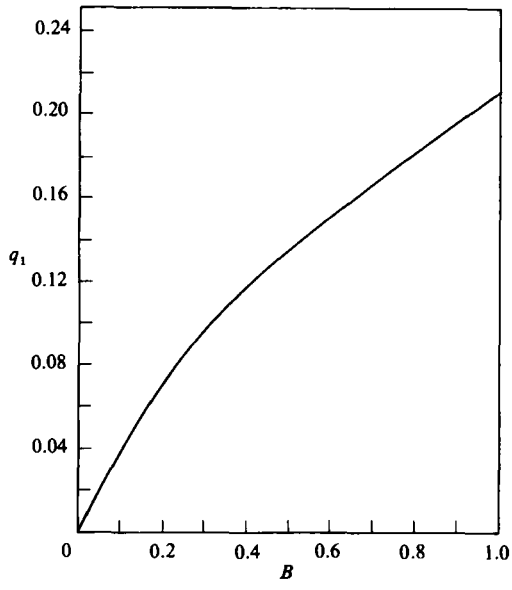

FIGURE 18. Exchange rate $q_1 = -q_2$ without barotropic flow as a function of width ratio B.

and shown in figure 17. It is interesting that the barotropic flow speed at which two-layer control is lost turns out to be a quite sensitive function of B when the relative decrease in channel width at the contraction is small (i.e. B close to 1). The dependence of flow rate q_i on B without barotropic flow is shown in figure 18.

Our idealized example includes an infinitely deep channel on each side of the sill. This approximation will often be good, but the modification for finite depth or a stagnant third layer (see figure 12) is readily included. Let the relative channel depth H be defined as

$$H = \frac{y_{1o}+y_{2o}}{y_{1e}+y_{2e}}, \tag{27}$$

then the exit condition is

$$\frac{u_{1e}^2}{y_{1e}}+\frac{u_{2e}^2}{y_{2e}} = 1. \tag{16d''}$$

An additional continuity equation for the lower layer is also required:

$$u_{2o}\,y_{2o} = u_{2e}\,y_{2e}\,B, \tag{16e''}$$

and the finite speed of the lower layer must now be included in the energy equation:

$$\tfrac{1}{2}(u_{1o}^2-u_{2o}^2)-y_{1o} = \tfrac{1}{2}(u_{1e}-u_{2e})-y_{1e}. \tag{16c''}$$

Solutions may then be found in the same way for equations (16a, b, c'', d'', e', e'', f) and (25) and (27). The effect of a finite depth through the exit will be to raise slightly the exchange rates found previously. However, the essential results will not change significantly.

Just as for flow through a contraction alone, submaximal solutions in which a reservoir condition influences the control, are also possible for flows over sills. The calculation will be identical to that discussed in Armi & Farmer (1986) (equations (A 2a–d) with y_{2r} replaced by $1-y_{1r}$). Submaximal flows occur whenever the reservoir interface depth on the right $(y_{1r})_R$ is deeper than $\frac{3}{2}$ its depth at the exit control y_{1e}.

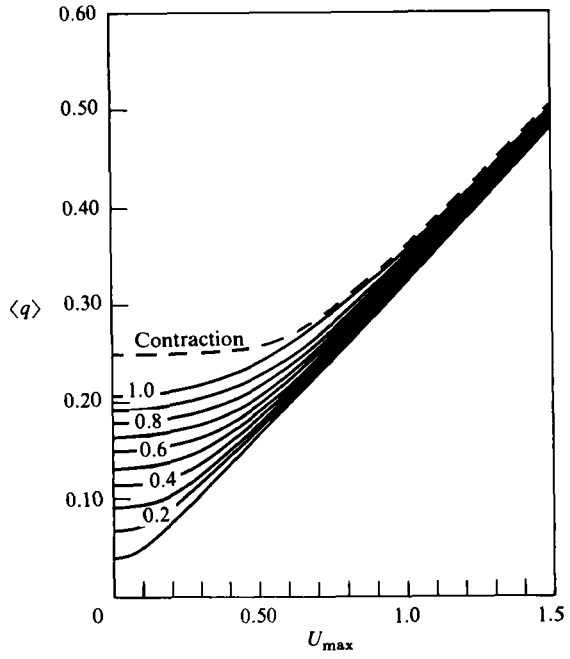

FIGURE 19. Exchange rate $\langle q \rangle$ averaged over a tidal cycle of amplitude U_{max} for different values of the width ratio B. The dashed line shows $\langle q \rangle$ for a contraction with depth equal to the depth of the sill crest.

(This arises from the control condition $F_1^2 = 1$ for a single-layer flow, since we assume $F_2^2 = 0$ at the exit.) The limiting left-hand reservoir condition for exchange controlled at the sill is that the reservoir interface be deeper than $\frac{3}{2}y_{1e}$. If the left-hand reservoir interface depth is between $\frac{3}{2}y_{1e}$ and $(y_{1r})_R$, control is lost at the sill and submaximal control of the upper layer occurs at the exit b_e. The exchange rate of the deeper layer is then specified by the continuity equation. For a sufficiently shallow interface in the reservoir to the left and an appropriate positive barotropic component, both layers flow in the same direction. This is an example of the 'reverse flow' discussed by Armi & Farmer (1986), for which $U_0 > U_{R+}$; a similar effect is possible for negative barotropic flow.

8. Periodic forcing

The influence of periodic forcing, such as that produced by tidal effects, can be found by integration of (16*a–b*) and (16*f*'), for given values of B and tidal amplitude U_{max}, together with the appropriate flow rates for intermediate and strong flows. We restrict attention to quasi-steady flows for which the time taken for long-wave adjustments to travel between the sill (b_0) and the contraction or exit (b_e) is significantly less than a quarter tidal period.

The results of the integrations are shown in figure 19, where we have also shown for comparison the corresponding periodically averaged exchange curve for a contraction only. As the relative contraction width B decreases, the nonlinear portion of the average exchange curve shown in figure 19 decreases. This effect is a consequence of the reduced range of U_0 over which internal hydraulic control is retained for smaller values of B. For $U_{max} > 1$, the curve approaches a straight line

of slope π^{-1}. The effect of the internal control is always to reduce the influence of the periodic flow on the average two-way exchange. As shown in §4 figure 5, the dependence of flow-rate curves on barotropic flow for the sill is nonlinear, while for the contraction alone it is nearly linear. This distinction accounts for the fact that the influence of moderate tidal flow through a contraction is negligible, but is significant over a sill and through a combination of a sill and contraction.

9. Discussion and application

Two-way hydraulically controlled exchange over a sill differs significantly from the corresponding problem of two-way flow through a contraction. The control at the sill crest acts primarily through the deeper layer into which it protrudes, and only indirectly controls the surface layer. The interface is deeper over the sill crest and the lower layer flows more rapidly than in the corresponding contraction example, but the exchange is significantly less. The application of Stommel & Farmer's (1953) result to exchange over a sill is therefore incorrect.

The asymmetry of the sill-control problem is especially apparent for barotropic flows. Two-layer flow in which only a single layer moves, i.e. intermediate flow, can only occur for negative barotropic components. When a strait includes both a sill and a separate contraction, the contraction influences the sill exchange only if it lies between the sill and the reservoir containing the denser fluid. The effect of positive barotropic flow is sensitive to the relative width of the contraction; the narrower the contraction, the smaller is the positive barotropic flow required to overcome hydraulic control at the sill and create a single-layer flow. The differences between these various examples is also apparent when integrated over periodic forcing (figure 18).

An illustrative example of many of the features developed in this analysis is provided by the Strait of Gibraltar. A recent photograph taken from the space-shuttle is shown in figure 20(*b*) (plate 1) together with a sketch emphasizing prominent features of the image as well as the location of the sill and of the narrowest section (figure 20*a*).

The effect of evaporation from the Mediterranean exceeds that of river discharge and precipitation, producing relatively saline water that passes out through the strait beneath the less dense Atlantic water flowing in along the surface. The strait therefore separates a reservoir of dense water, lying on the right-hand side in our convention, from less dense water on the left ($\Delta\rho/\rho_2 \approx 0.002$). It is characterized both by a sill (Camarinal) of depth $\simeq$ 280 m, width $\simeq$ 12 km, and also by a horizontal contraction of depth 900 m and width 9 km to the east at Tarifa. The strait is therefore an example of the type shown in figure 13 in which both a sill and a separate contraction control the exchange; the relative width of the contraction is $B = 0.6$–0.8. A second and slightly deeper sill ($\simeq$ 300 m) lies to the west of the first sill, separated by Tangier Basin (figure 20).

Rotation produces an observed mean tilt of the interface, which is 30–50 m, depending on position in the channel. Given typical pycnocline depths of order 50–150 m, rotation is likely to influence behaviour of the hydraulic controls, but it will not be a dominant effect and should not alter the essential results discussed here.

Flow through the strait is modulated by strong tides and also by meteorological effects. Drawing from the extensive data presented by Lacombe & Richez (1982), Armi & Farmer (1985) calculated Froude numbers at various points along the channel. Except for a short portion of the tidal cycle when the surface layer may

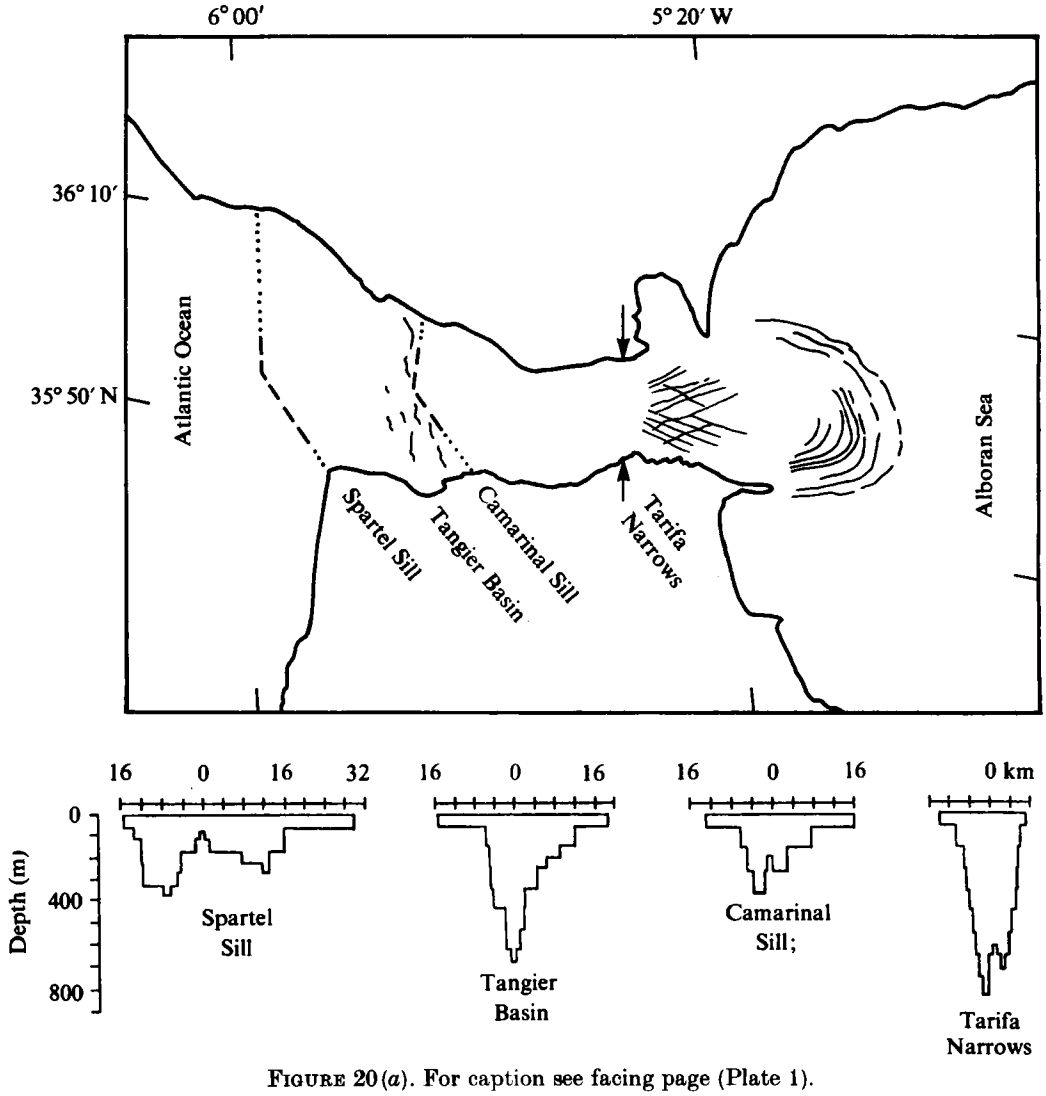

FIGURE 20(*a*). For caption see facing page (Plate 1).

(b)

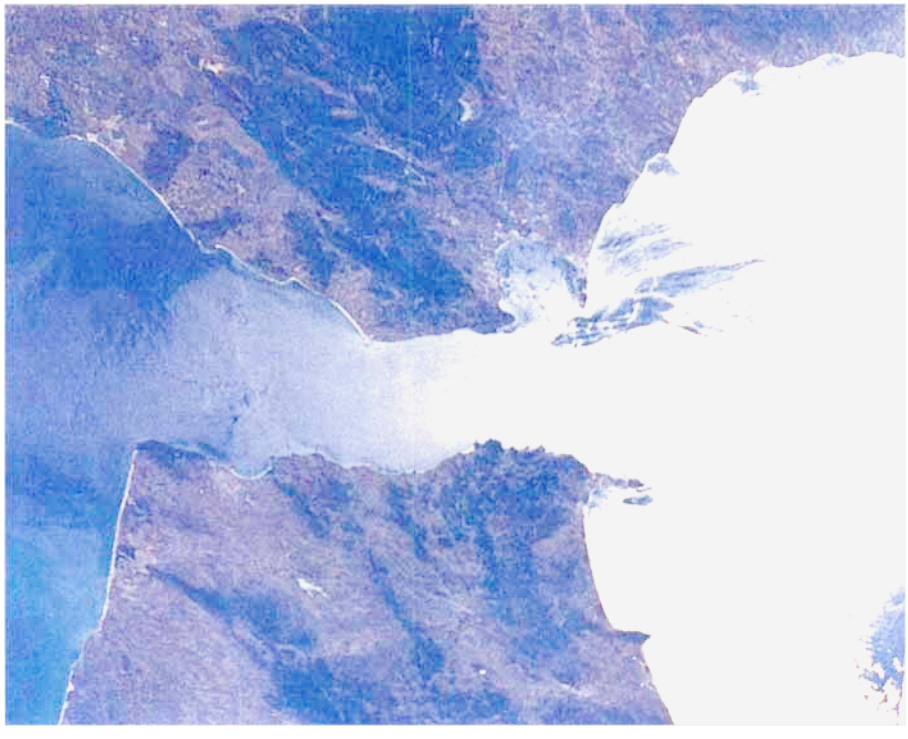

FIGURE 20. *(a)* Map showing essential geographic features as well as sketches of the principal surface manifestations apparent in the photograph above. Clearly visible in the image are the surface effects of the internal undular bore radiating into the Alboran Sea and of the internal hydraulic jump connecting flow over Camarinal Sill to Tangier Basin. *(b)* Photograph of Gibraltar Strait taken from the space shuttle in October 1984. (Photo courtesy of Paul Scully-Power, National Aeronautics and Space Administration, Lyndon B. Johnson Space Centre, Houston, Texas 77058, Photo S-17-34-080). Interfacial features associated with the internal hydraulics show up clearly as modulations in the sun glitter from the sea surface. The photograph was taken at 1221.38 h GMT, 11 October 1984. Low water (0.2 m) at Gibraltar was at 0749 h GMT, high tide (1.0 m) at 1416 h GMT.

disappear near the contraction and fronts form suddenly, the flow to the east of the narrowest section is supercritical ($F_1^2 > 1$, $F_2^2 \simeq 0$). West of the sill at Spartel, during the outflowing tide the deep layer forms a thin supercritical flow ($F_2^2 > 1$) leaving Tangier Basin. Flow through the Strait of Gibraltar therefore has the asymmetric structure of maximal two-way exchange sketched in figure 13, although subject to significant modulation by the tides. A long internal wave can travel between Camarinal Sill and Tarifa Narrows in 1.5 h; for the 12.5 h semi-diurnal tide the quasi-steady assumption is therefore only approximate.

The underlying asymmetry of the response to tidal flow, discussed in §§4, 5, is also evident in figure 20. The semi-circular banded structure emanating from the eastern end of the Strait is the surface manifestation of an internal undular bore. There are many reports of this feature (Kinder 1984; Ziegenbein 1969, 1970), which originates in the release of the energy associated with deformation of the interface downstream of the sill crest (figure 13) as the outflowing tide slackens and subsequently evolves into a train of nonlinear internal waves. Ziegenbein (1969) reports that the bore enters the Alboran Sea 5–6 hours after high water. The photograph in figure 20 was taken approximately 10 hours after the previous high water, which is consistent with the bore's appearance well inside the Alboran Sea.

The interface in Tangier Basin is shallower than $\frac{3}{2}y_{1e}$ (Tarifa Narrows) during part of the tidal cycle (Armi & Farmer 1985 figure 4), thus permitting submaximal exchange. Armi & Farmer (1985 figure 5) show that during a portion of the inflowing tide the lower layer reverses; thus the tide forces the exchange past the submaximal regime and into reverse flow ($U_0 > U_{R+}$). However, this inflow need not be critical and no internal undular bore has been reported travelling westwards out of the Strait, despite extensive observations.

The sudden appearance of fronts near the contraction at certain stages of the tide is consistent with negative barotropic flow through the transition speed $U_0 = -(\frac{2}{3})^{\frac{3}{2}}$. Thus the barotropic component during the outflowing tide can be intermediate, in the sense described in §5. Downstream of Camarinal Sill (figure 20) there are other surface features. These are consistent with the expected surface manifestation of the plunging supercritical layer and internal hydraulic jump required to match the outflow to the reservoir condition in Tangier Basin. The photograph was taken 2 hours before high water, at which time a strong outflow is observed over the sill (see figure 5 in Armi & Farmer 1985).

One other feature of the photograph in figure 20 is explainable in terms of the internal hydraulics. Just east of the narrowest section of the contraction an oblique wave pattern is observable. This is apparently the surface manifestation of an oblique internal wave pattern formed in the supercritical flow east of the narrowest section; similar waves are observed in open-channel flows (Henderson 1966 pp. 239–250 figures 7–9) and in gas flow through a nozzle (Prandtl 1952 pp. 275–277, figure 4.16).

The exchange through the Strait of Gibraltar is therefore maximal for a significant portion, but not for all, of the tidal cycle. The hydraulic processes which limit flow through the Strait influence the larger-scale properties of the Mediterranean Sea and, together with the net evaporation rate, determine the salinity of the outflow. Bryden & Stommel (1984) recently estimated the exchange rates in this way, together with the corresponding outflow salinity for the Strait of Gibraltar, although their use of an interface depth over the sill based on (15) rather than (14), and their neglect of tidal forcing, limits the applicability of their result. While further observations are needed to resolve the details of these processes, it is clear that both the combined influence of the contraction and the two sills, and also effects of the various classes

of barotropic flows discussed earlier will determine the magnitude of the exchange between the Mediterranean and the Atlantic Ocean.

We are indebted to Grace Kamitakahara-King and Sharon Yamasaki for carrying out the numerical calculations and to Dr Donald Booth for his assistance with the numerical analysis. We are also indebted to two reviewers, David Wilkinson and an anonymous one, for many helpful comments. All calculations were done independently at the Institute of Ocean Sciences and Scripps Institution of Oceanography. This work received partial support from the Office of Naval Research.

REFERENCES

ANATI, D. A. 1976 Balances and transports in the Red Sea and the Gulf of Elat ('Aqaba). *Israel J. Earth-Sciences* **L5**, 104–110.

ARMI, L. 1986 The hydraulics of two flowing layers with different densities. *J. Fluid Mech.* **163**, 27–58.

ARMI, L. & FARMER, D. M. 1985 The internal hydraulics of the Strait of Gibraltar and associated sills and narrows. *Oceanologica Acta* **8**. 37–46.

ARMI, L. & FARMER, D. M. 1986 Maximal two-layer exchange through a contraction with barotropic net flow. *J. Fluid Mech.* **164**. 27–51.

BRYDEN, H. L. & STOMMEL, H. M. 1984 Limiting processes that determine basic features of the circulation in the Mediterranean Sea. *Oceanologica Acta* **7**, 289–296.

HENDERSON, F. M. 1966 *Open Channel Flow*. Macmillan. 522 pp.

HOGG, N. G. 1985 Multilayer hydraulic control with application to the Alboran Sea circulation. *J. Phys. Oceanog.* **15**, 484–466.

KINDER, T. H. 1984 Net mass transport by internal waves near the Strait of Gibraltar. *Geophys. Res. Letters* **11** (10), 987–990.

LACOMBE, H. & RICHEZ, C. 1982 The regime of the Strait of Gibraltar. In *Hydrodynamics of Semi-Enclosed Seas* (ed. J. C. J. Nihoul). Elsevier Oceanography Series, vol. 34, pp. 13–73.

MURRAY, S. P., HECHT, A. & BABCOCK, A. 1984 On the mean flow in the Tiran Strait in winter. *J. Mar. Res.* **42**, 265–287.

PRANDTL, L. 1952 *Essentials of Fluid Dynamics*. Blackie and Sons. 452 pp.

STIGEBRANDT, A. 1977 On the effect of barotropic current fluctuations on the two-layer transport capacity of a constriction. *J. Phys. Oceanog.* **7**, 118–122.

STOMMEL, H. & FARMER, H. G. 1952 Abrupt change in width in two-layer open channel flow. *J. Mar. Res.* **11**, 205–214.

STOMMEL, H. & FARMER, H. G. 1953 Control of salinity in an estuary by a transition. *J. Mar. Res.* **12**, 13–20.

TURNER, J. S. 1973 *Buoyancy effects in fluids*. Cambridge University Press. 367 pp.

ZIEGENBEIN, J. 1969 Short interval waves in the Strait of Gibraltar. *Deep-Sea Res.* **16**, 479–487.

ZIEGENBEIN, J. 1970 Spatial observations of short internal waves in the Strait of Gibraltar. *Deep-Sea Res.* **17**, 867–875.